J Mater Sci (2023) 58:9486–9501

Composites & nanocomposites

Synergies of material and geometrical non-linearities allow for the tuning of damping properties of functionally graded composite materials

Jacopo Romanò[1,2,*], Lorenzo Garavaglia[1], Fabio Lazzari[1,2], Francesco Volontè[1,2], Francesco Briatico Vangosa[2], and Simone Pittaccio[1]

[1] Institute of Condensed Matter Chemistry and Technologies for Energy (CNR-ICMATE), National Research Council of Italy, Via Previati 1/E, 23900 Lecco, Italy
[2] Department of Chemistry and Materials Engineering (DCMIC), Politecnico di Milano, Milan, Italy

Received: 30 January 2023
Accepted: 16 May 2023
Published online: 8 June 2023

ABSTRACT

In this study, we present an alternative fabrication technique to obtain functionally graded polymer–metal composites. The aim is to obtain a composite material with a graded damping factor, which is provided by the presence of pseudoelastic nickel–titanium (NiTi) fibres within an epoxy resin matrix. A preliminary dynamic mechanical characterisation of the NiTi wire revealed a pre-strain dependency of its damping factor. By fabricating wires with curved geometries in the free state, we were able to obtain fibres with a graded level of pre-strain when straightened. This feature in turn imparts a graded damping response. When encapsulating the straightened fibres in an epoxy resin, the graded damping response is transferred to the composite.

Introduction

Functionally graded materials (FGMs) are a class of materials characterised by a continuous or smooth gradient of a certain property (mechanical, thermal, tribological,…), along a particular direction [1]. This continuous grading can be beneficial for applications in several engineering fields, such as aerospace [2, 3], energy and sensors [4] and biomedical [5]. Generally, the main advantage consists in the possibility of integrating solutions to spatially changing structural/functional requirements within fewer elements, thus minimising the number of components, mechanical transmissions and the efficiency losses [6]. The various methods typically employed to fabricate FGMs revolve around creating a graded variation in the meso- or micro-structure, which will then affect the material behaviour. Such methods include centrifugal methods [7], powder metallurgy [8], vapour deposition [9], infiltration [10], thermal spray [11] and electrodeposition [12]. In more recent years, particular interest has been given to additive manufacturing and its potential to create structured FGMs

Handling Editor: Mohammad Naraghi.

Address correspondence to E-mail: jacopo.romano@icmate.cnr.it

https://doi.org/10.1007/s10853-023-08612-2

[13]. Despite these recent advances, the study of new fabrication processes and their effects on the behaviour of FGMs remains one of the current challenges in the research of this class of materials [14].

When designing novel fabrication strategies for FGMs, it can be useful to take inspiration from nature, where shape and material properties are closely interrelated, and oftentimes, the properties of biological tissues are heavily dependent on their structure/morphology and microstructure. At the same time, the shape of living organisms is the result of centuries of evolution aimed at optimally fulfilling a given function with the minimum expense of building material and energy [15]. This kind of synergistic approach between material shape and function could be extremely beneficial when applied to the field of FGMs.

In the present study, we investigate the possibility to exploit synergies between material and geometrical non-linearities in order to obtain a functionally graded polymer/metal composite material. The function whose grading we seek to control is damping, the capacity from the material to dissipate incoming mechanical energy. This will be carried out by including nearly-equiatomic NiTi alloy wires, endowed with specific shape-set morphology. This alloy is well known in the literature for its pseudoelastic behaviour and the shape memory effect [16]. There are examples of FGMs that utilise this alloy; however, all these studies rely on conventional fabrication methods, such as those previously mentioned [17, 18] or plasma sintering [19] to obtain the property gradient. Our study aims to investigate a new approach (Curvilinear pre-straining—CPS), based on exploiting the straightening of curved geometries, to obtain a gradient in the damping factor of our composite material. This approach is made possible by the pre-strain dependency that we observed for the damping factor in NiTi, and the possibility to strengthen the effect, using dedicated heat treatments [20]. Based on that evidence, we came up with the idea to shape-set wires in a curvilinear shape, then straighten them and include them within an epoxy matrix, in order to produce and maintain a non-uniform level of pre-strain along the length of the fibre. When evaluating the dynamic response of the resulting composite material, we found that this method successfully caused a predictable and controllable grading of the damping factor along the length of the composite.

The study is organised as follows:

First, dynamic mechanical analysis of the metallic component (wires) is carried out in order to investigate the various dependencies (temperature, frequency, amplitude and pre-strain level). Having confirmed that the damping factor of the metallic material is pre-strain dependent, we then seek to use curved geometries to introduce a continuous pre-strain modulation along the length of the wire: by shape-setting the wire into a non-straight geometry (in their stress-free configuration), we can impart a pre-strain distribution to the wire by a straightening it post-treatment. The distribution will depend on the initial stress-free geometry. Three different curved geometries are selected to prove the validity of the CPS approach. The curved wires are straightened, and the straight configuration is held in an *ad hoc* fixture. Meanwhile, epoxy resin is used to encapsulate the wires and allowed to cure. This will allow the resin, once the fixture is removed, to maintain the wires pre-strain level. Dynamic mechanical analysis (DMA) is then carried out on the polymer/metal samples to check the validity of our approach.

The structure of the paper is as follows:

In the Materials and Methods section, we provide an overview of the constituent components of the composite (NiTi wire and epoxy resin), their processing parameters and the methods used to carry out the mechanical characterisation of the metallic wire. We then describe the methods used to predict the pre-strain distribution along the length of the straightened wire from the knowledge of their initial curved shape. Finally, we provide the methods for the dynamical mechanical analysis of the samples.

In the Results section, we first present the dynamic mechanical characterisation of the metallic wire, followed by that of the composite structures.

Finally, we discuss these results and draw our conclusions.

Materials and methods

Material selection and processing

Commercial NiTi wire with a nominal composition Ni50.6-Ti49.4 (1.2 mm diameter) was cold drawn to a nominal diameter of 0.4 mm, with a residual cold-work level of 43% (cross-section reduction).

Part of the wire underwent a short duration (20 s) pre-treatment at 550 °C, in order to increase its mechanical hysteresis as described in [20], and was then straight-annealed at 435 °C for 400 s. Both treatments were carried out in an electric kiln, and the samples were water quenched at the end of each treatment. The stress–strain response of the wire, as well as calorimetric analysis highlighting its transformation temperatures can be found in [20]. The straight wires thus obtained underwent dynamic mechanical characterisation.

The rest of the wire was cut into segments of appropriate length, set in jigs *ad-hoc* designed to impart specific curvature and underwent the same short-duration pre-treatment, followed by thermal annealing. Three different types of jigs (Fig. 1(1)) were used to shape-set the wire into three different non-straight geometries, selected as described in "Selection of curvilinear geometries" section. These curved wires were used for the fabrication of the composite samples.

Commercial, bicomponent epoxy resin (EC57/K21, Elantas Europe s.r.l., Hamburg, Germany) was selected because of its good mechanical and chemical compatibility with NiTi [21]. The resin (declared glass-transition temperature $Tg \approx 125$ °C) was cast in a silicone mould, and a two-step curing was carried out: first 24 h at room temperature, followed by 15 h at 80 °C.

The silicone mould was designed to allow the fabrication of plain epoxy samples, as well as the metal-epoxy composites. Both composites and plain samples are square-based (5 mm-side) prisms, of 50 mm length. Each final polymer/metal sample contains a single pre-strained NiTi wire.

The fabrication process of the samples is summarised in Fig. 1. The curved wires are shape set, and then inserted in a silicone mould, where the curing of the epoxy resin will take place (Fig. 1(2)). This partially straightens them, but to reach the desired pre-strain level, a subsequent step is required. The silicone mould is contained within a metallic jig design to apply and maintain the desired pre-strain level during epoxy curing. Both the pitch (1 mm) in the threading of the fixture bars of the jig, and the length of the straightened wire are known. By turning the nuts (highlighted in Fig. 1(3)) accordingly, it is possible to set the pre-strain of the wires to the desired value. The resin is then poured in the mould and left to cure as previously discussed.

Dynamic mechanical characterisation of the NiTi wire

Dynamic mechanical characterisation of the NiTi wire was carried out on a dynamic tensile test machine (ElectroPuls E3000, Instron, Norwood, Massachusetts, USA). First, the wire was pulled quasi-statically (0.01%/s) up to a set level of pre-strain (ε_{PS}, equal to 1%, 2%, 3% while loading the wire, then 2% and 1% while unloading). The gauge length was 40 mm. In the results, tests are labelled based on the level of pre-strain followed by the letter L for the tests performed during loading, and U for those performed during unloading, as summarised in Fig. 2.

Figure 1 Fabrication process of the composite samples. **1** The wires are shape set with custom jigs and subjected to thermal annealing. **2** The wires are put in a silicone mould within a metallic jig. This already partially straightens them. **3** The wires are blocked with metallic crimps, to fix them to the jig, and are straightened to the desired level of pre-strain. The nuts used to apply the pre-strain are highlighted in red. The other nuts remain fixed. The resin is then added and let to cure, while the strain is maintained.

At each of these pre-strain levels, an additional sinusoidally varying strain was applied to the wire.

$$\varepsilon(t) = \left(\varepsilon_{PS} + \frac{\Delta\varepsilon}{2}\right)\sin(2\pi ft) \quad (1)$$

Three different strain amplitudes ($\Delta\varepsilon$ equal to 0.1%, 0.5%, 1%) were tested. For each amplitude, a frequency sweep between 0.1 and 20 Hz was tested. This entire procedure was repeated at the temperatures of 15 °C, 25 °C, 45 °C and 70 °C.

From the measured stress σ_0, the storage (E') and loss (E'') moduli were calculated, respectively, as:

$$E' = \frac{\sigma_0}{\varepsilon_0}\cos\delta \quad (2)$$

$$E'' = \frac{\sigma_0}{\varepsilon_0}\sin\delta \quad (3)$$

where **d** is the phase delay between the applied strain and the measured stress.

The damping factor η of the material was calculated as:

$$\eta = \frac{E''}{E'} \quad (4)$$

The hysteresis area of the partial cycles was also calculated as the difference between the areas under the loading and unloading plateaux.

Selection of curvilinear geometries

The pre-strain distribution along the length of the straightened wire was predicted starting from the analytical expression describing the (planar) curvilinear shape to be imparted to the central axis, and the (constant) diameter of the wire. As the curvature is in general variable, let us consider a local polar system of coordinates referred to some point along the axis (Fig. 3). Assuming a circular cross-section of diameter d and a local radius of curvature of the central axis ρ_b, it is possible [22] to obtain an expression for the radius of curvature of the neutral axis as:

$$\rho_b = \frac{d^2}{4\left(2\rho_b - \sqrt{4\rho_b^2 - d^2}\right)} \neq \rho_n \quad (5)$$

Be AB is a generic fibre in an infinitesimal portion of the wire, and CD is the fibre corresponding to the neutral axis. Be y is the distance between the two fibres. Assuming a perfect straightening of the wire,

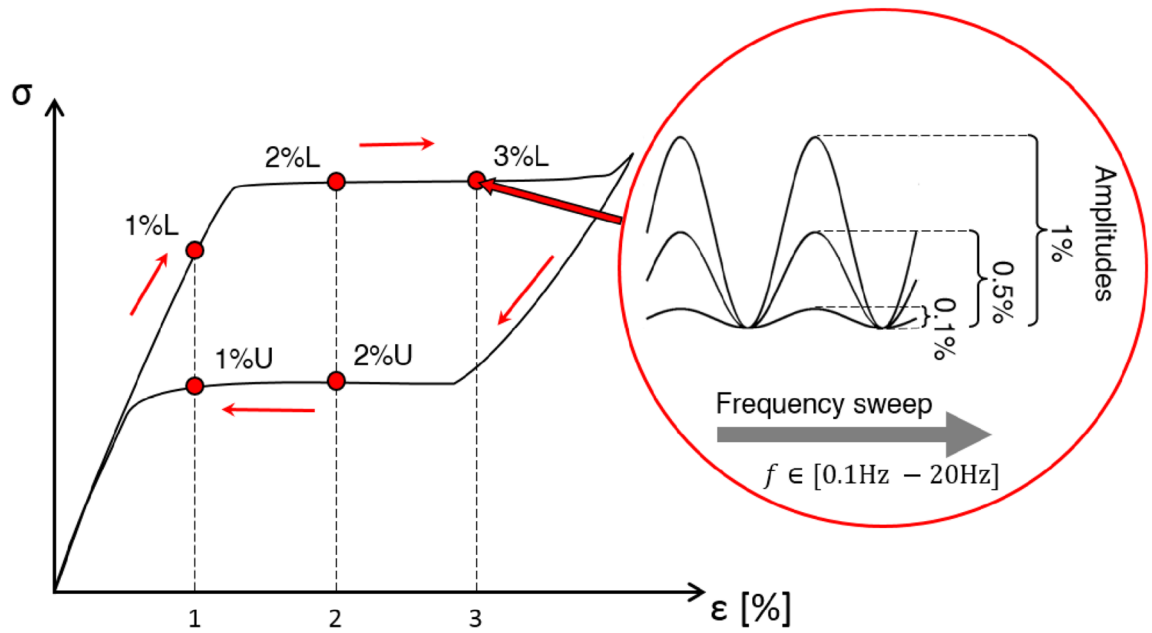

Figure 2 Experimental method for the dynamic testing of the NiTi wire. A quasi-static load is applied up to a certain level of pre-strain (1%, 2%, etc.). Once this level is reached and while maintaining it, an oscillating strain is applied, sweeping a frequency range between 0.1 and 20 Hz, at three different amplitudes. After reaching 3%, the pre-strain is reduced, and the 2% and 3% points are tested on the lower level of the pseudoelastic plateaux. The entire process is then repeated at higher temperatures, sweeping a temperature range from 15 to 70 °C.

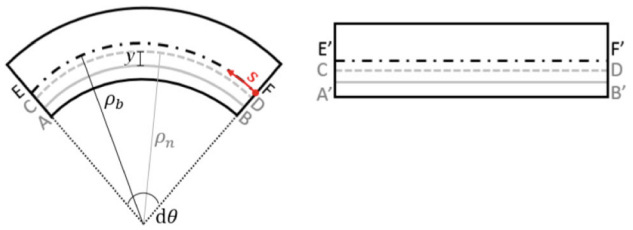

Figure 3 Schematic representation of an infinitesimal portion of the wire with a given local curvature radius ρ_b. On the left, the shape-set, stress-free morphology; on the right the corresponding straightened configuration. Primed letters indicate the points on the straightened wire corresponding to the points labelled with the same unprimed letters in the curved configuration. Radius ρ_n marks the local radius of curvature of the neutral axis, which is not central for curved beams, albeit of symmetrical cross-section.

CD will keep the same length, while the fibre AB will change its length to A′B′, where A′B′ = CD. All these lengths can be calculated from the radii and the angle between the ends of the wire portion. We can thus write the strain distribution as a function of the axial coordinate s running along the wire central axis:

$$\varepsilon(s,y) = \frac{A'B' - AB}{AB} = \frac{CD - AB}{AB} = \frac{\mathrm{d}\theta\rho_n - \mathrm{d}\theta(\rho_n - y)}{\mathrm{d}\theta(\rho_n - y)} = \frac{y}{(\rho_n(s) - y)} \tag{6}$$

Three different planar curvilinear geometries (Fig. 4) were selected: a semicircular shape (*C*) of constant nonzero curvature, an Archimedean spiral (*S*) with monotonously changing curvature, and a more complex shape (*D*) with a double change in curvature. The rationale behind the selection of these shapes is based on the requirement that the grading of the damping response should be testable against different characteristics of the nonlinear geometries. For instance, symmetry and non-monotonicity were both considered parameters of interest. The first geometry, C, is based on a semicircle, has a constant, nonzero curvature, and is both symmetrical and monotone. The second, S, is based on an Archimedean spiral, and is asymmetrical but still monotone. The final shape, D, has a non-monotonic but symmetrical curvature.

Their analytical expressions, given for straightforwardness in polar coordinates, is:

$$\begin{aligned} \text{C:} &\rho_\mathrm{b} = r_\mathrm{C} \\ \text{S:} &\rho_b = r_\mathrm{S}\theta \\ \text{D} : &\rho_\mathrm{b} = k_\mathrm{D}\cos(2\theta) + r_\mathrm{D} \end{aligned} \tag{7}$$

where r_C, r_S,k_D and r_D are constants, and $\theta \in [0, \pi]$.

The respective axial coordinates for the three geometries can be expressed as functions of the same parameter θ as follows:

$$\begin{aligned} \text{C: } &s(\theta) = r_\mathrm{C}^2\theta \\ \text{S: } &s(\theta) = r_\mathrm{S}^2\theta\left(1 + \frac{\theta^2}{3}\right) \\ \text{D: } &s(\theta) = (r_\mathrm{D}^2 + k_\mathrm{D}^2)\theta + r_\mathrm{D}k_\mathrm{D}\sin(2\theta) \end{aligned} \tag{8}$$

For the fabrication of the samples, these curves were engraved in aluminium to obtain the corresponding jigs, and a straight portion directed as the local tangent vector was added to the two ends, to provide two end-tails of the wire that could be held while applying the pre-strain through the fixture frame (see Fig. 1(1)).

Mechanical testing of the composites

Pull-out tests were carried out on a mechanical universal test machine (ElectroPuls E3000, Instron, Norwood, Massachussetts, USA). Sample holders were designed for the test and 3D printed with 3D printer Raise 3D N2 Plus (Raise 3D, Irvine, California, USA), using a polylactic acid (PLA)-based filament (Alfaplus, Filoalfa, Turin, Italy). The holders (Fig. 2(6)) were designed as hollow cylinders with outer and inner diameter, respectively, of 13 mm and 10 mm, and a height of 23 mm. 65 mm long straight-annealed NiTi wires were aligned with the central axis of the cylindrical holders. Epoxy resin was then added and allowed to cure as described in "Material selection and processing" section. Twelve samples were fabricated and tested by applying a quasi-static displacement (0.01 mm/s, corresponding to an apparent strain of 0.0005/s, calculated on an interface length L of 20 mm) to the wire until interface failure.

Mechanical tests were then conducted (DMA Q800, TA Instruments, New Castle (DE), USA) on the polymer–metal composite samples. The polymer–metal samples were named according to the stress-free, curved wire shape (C, S and D, as described in the previous section). A plain epoxy sample (P) was also considered.

Dynamic analysis was carried out on all the samples, applying a cyclic displacement with an amplitude of 10 μm. These tests were carried out in a frequency range between 0.1 and 5 Hz, and a temperature sweep between 20 and 90 °C. Different regions of the samples corresponding to specific portions of the straightened fibres (the sample was

constrained in the regions indicated by roman numbers, as shown in Fig. 5), were probed in this way. Note that, in general, they correspond to different radii of curvature of the initial configuration. The distance (L = 17 mm) at which the load (F) was applied was kept constant, regardless of the zone (Fig. 5). Particular care was taken to apply the load on the side of the compressed fibres, so that the load would be added to the pre-tension of the metallic fibres, and not subtracted. The maximum bending stress was calculated as an effective stress considering the whole sample isotropic and homogeneous.

Statistical analysis

The results of the mechanical tests were grouped according to the different dependencies investigated, as outlined in "Dynamic mechanical characterisation of the NiTi wire" section. These groups were characterised by different frequencies, amplitudes, temperatures and pre-strain levels. N-way analysis of variance (ANOVA) was used to determine statistically significant differences in damping through multiple comparisons including the temperature (degrees of freedom dof = 3), the amplitude (dof = 2), frequency (dof = 11) factors and the temperature*amplitude (dof = 6), temperature*frequency (dof = 33) and amplitude*frequency (dof = 22) interactions. Significance was established for $p < 0.01$.

Student t test was used to compare the average damping factor at different temperatures, once again with $p < 0.01$. Statistical data are provided as supplementary information (Online Resource 1).

Results

Mechanical characterisation of NiTi wire

The results of the dynamic mechanical tests on the NiTi wire can be seen in Fig. 6.

No significant combined effects of the frequency and either temperature or amplitude were detected. When restricting the observation to the 0.1–2.5 Hz range, the frequency dependency of η is significant (p = 2.5e-10): the damping factor is higher at low frequencies. For frequencies higher than 5 Hz, frequency no longer has a significant effect.

The effects of strain amplitude are significant (p = 2.3e-8): as strain amplitude increases, the average damping factor also increases. The difference between the various pre-strain levels becomes significant (p = 1.8e-4) at 1% amplitude, while for 0.1% and 0.5%, the within group variation is not significant.

At 1% amplitude, we can observe that the average damping factor measured at the "extreme" levels of pre-strain (i.e. the lowest, 1% pre-strain reached while loading, from here on called 1%L, and highest, 3%L) is lower than at intermediate pre-strains. Moreover, there is a clear difference between the damping factors measured at the same pre-strain during loading and unloading, with the greatest difference between damping factors being ~ 0.1 (1%L vs 1%U). All these observations hold valid for all repeated experiments, regardless of the temperature.

The average damping factors are reported as functions of the different temperatures and amplitudes in Fig. 7. Temperature affects the damping

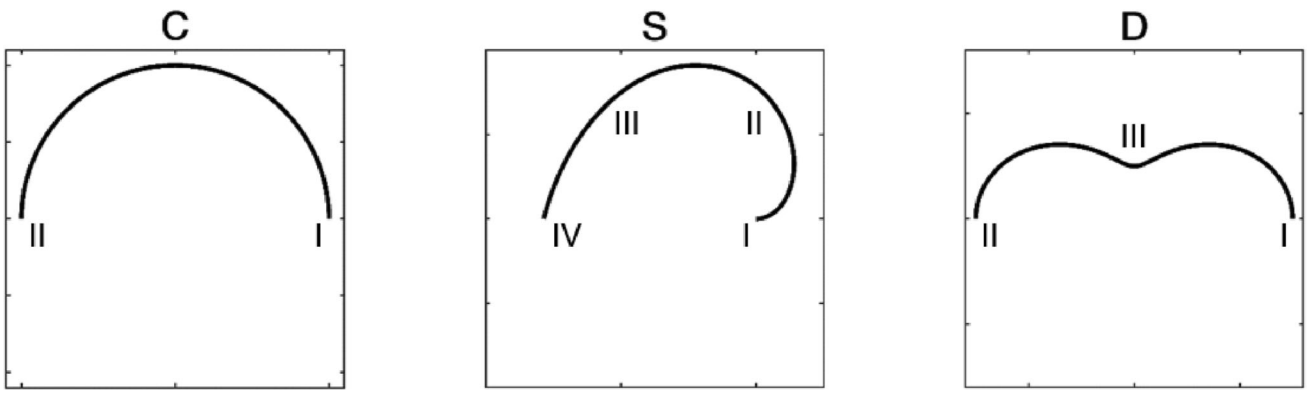

Figure 4 Plot in Cartesian coordinates of the three different geometries. The roman numbers denote the different zones where the samples are constrained during dynamic mechanical testing.

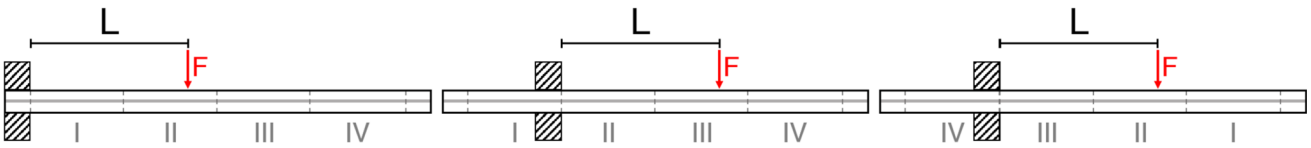

Figure 5 Schematic example of the experimental setup for the single cantilever tests for sample S. The different zones of the sample are marked with roman numbers. All samples have an initial and final region that allows holding the sample while testing the extreme zones. The length L at which the load F is applied is kept constant regardless of the zone, which is being probed.

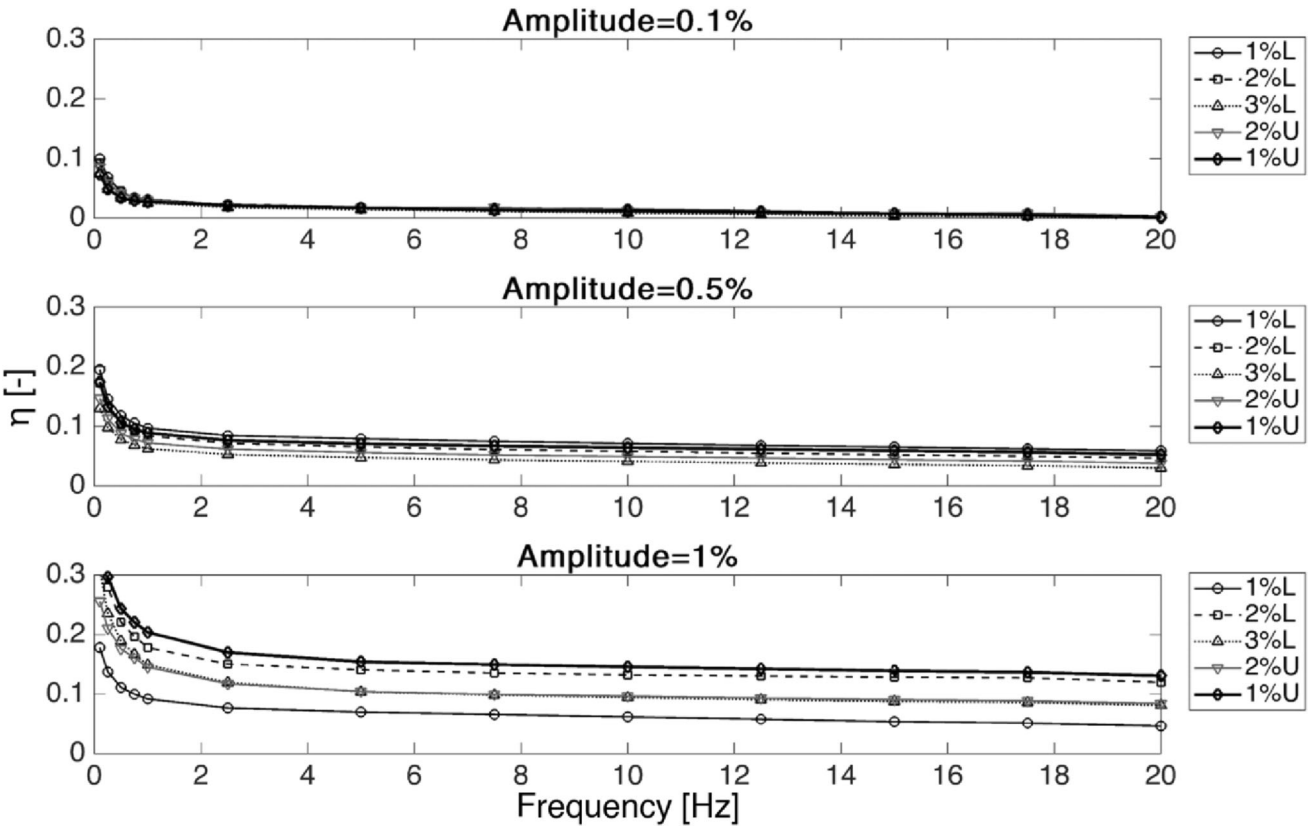

Figure 6 Damping factor of the NiTi wire as a function of the frequency and strain amplitude (0.1%, 0.5%, 1%). The different lines represent different levels of pre-strain. Measurements taken at temperature T = 25 °C.

factor (p = 5.5e-4), and a combined effect of temperature and strain amplitude on η is also observed (p = 1.04e-4). For low strain amplitudes, there appears to be no statistical effect of temperature on the damping factor. If the amplitude is sufficiently high, however, it becomes apparent ($p < 0.001$) that, as temperature increases, there is an exponential decrease in the damping factor, where $\eta = 0.28e^{-\frac{T+2.6}{24}}$ (R^2 = 0.9978).

Design of FGM

To obtain a grading of the mechanical properties of the wire along its length, three different geometries were considered. As described in "Selection of curvilinear geometries" section, the correlation between curvature and strain distribution allows us to predict the distribution of pre-strain along the wire.

From the results of "Mechanical characterisation of NiTi wire" section, we expect that the damping factor will vary for pre-strains in the range 0–3%. We have fabricated samples containing straightened wires with the C, S and D original shapes, setting the coefficients in Eq. 3 to obtain shape-determined pre-strains in excess of that range. This was done in order to assess the effect of applying CPS on NiTi. In detail, the values of the coefficients are r_C=10, r_S=5,=5 and

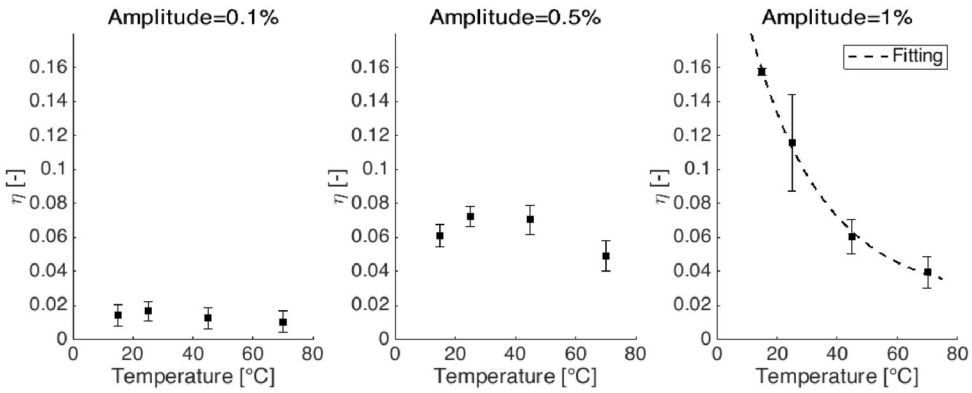

Figure 7 Temperature dependency of the damping factor at different levels of applied strain (0.1%, 0.5% and 1%). The effects of temperature are evident for higher strain amplitudes.

r_D=10. The results of this design step are found in Fig. 8.

The first geometry, referred to as C is semicircular, with a constant radius of curvature. We therefore expect a symmetrical behaviour of the composite, when tested on both ends. The absolute value of pre-strain is constant and ∼ 1.5% for both outermost and innermost fibres.

The second geometry (S) consists in an Archimedean spiral, which displays asymmetrical behaviour. The pre-strain decreases along the length of the wire and in regions I, II, III and IV (see "Mechanical testing of the composites" section), and is respectively equal to 3.5%, 2.5%, 1% and 0.1%.

The dual-curvature geometry (D) is symmetrical but has a central region with negative curvature. At the ends, the expected pre-strain is ∼ 3%, while in the central region it is ∼ 6%.

All the mentioned strains refer to the maximum values on outermost interior or exterior fibre. It should be noted that the compression and tension values are not symmetrical, since the neutral axis of the fibres does not correspond to its barycentric axis, as discussed in "Selection of curvilinear geometries" section. However, since the diameter of the fibre is very small when compared to its curvature radius, this difference is almost negligible (e.g., in the case of the circular fibre the maximum tensile and compressive strains are, respectively, ε_{traz} = 0.0203 and ε_{compr} = − 0.0197).

Mechanical characterisation of FGM

A representative pull-out test is shown in Fig. 9. The pseudoelastic behaviour of the metallic material needs to be taken into account when analysing these results. Usually, when a change in the first-order derivative of the force–displacement curve is detected, this indicates an interface failure, since a relative slip between the wire and the matrix is occurring. The force corresponding to this threshold is then used to calculate the interfacial shear strength τ_i [23]. In the case of a SMA wire, however, a change in the first-order derivative may simply indicate the start of the martensitic transformation. However, as shown in Fig. 9, it is still possible to distinguish between the various phenomena occurring during mechanical testing. Indeed, the pseudoelastic region and the slip region differ not only because the latter usually follows a sharp drop in force levels, indicating interface failure, but also because the pseudoelastic plateau has a slightly positive average first order derivative. The average derivative of the force measured, while the wire is slipping, on the other hand, is negative, since as the wire slips out of the sample there is less interface with the polymer, and the friction-induced shear force consequently decreases. This allowed to estimate the average value of interfacial shear strength as $\tau_i \cong 3.4 \pm 0.22$ MPa. The tests show that the interface strength is sufficiently high to allow the wire to almost fully undergo its phase transformation before failure, and since previous work in the literature also confirm the good adhesion between the two materials [21], the bonding between the NiTi alloy and the epoxy resin is considered satisfactory for the purpose of our work.

When comparing η of the different samples at 0.1 Hz (Fig. 10), the same symmetrical or asymmetrical behaviour already shown in the stress-displacement plot can be confirmed.

In general, as temperature approaches the *Tg* of the epoxy resin, there is an increase in η. Some samples, in particular C, D and S in zone III, also display a remarkably higher value of η at lower temperatures

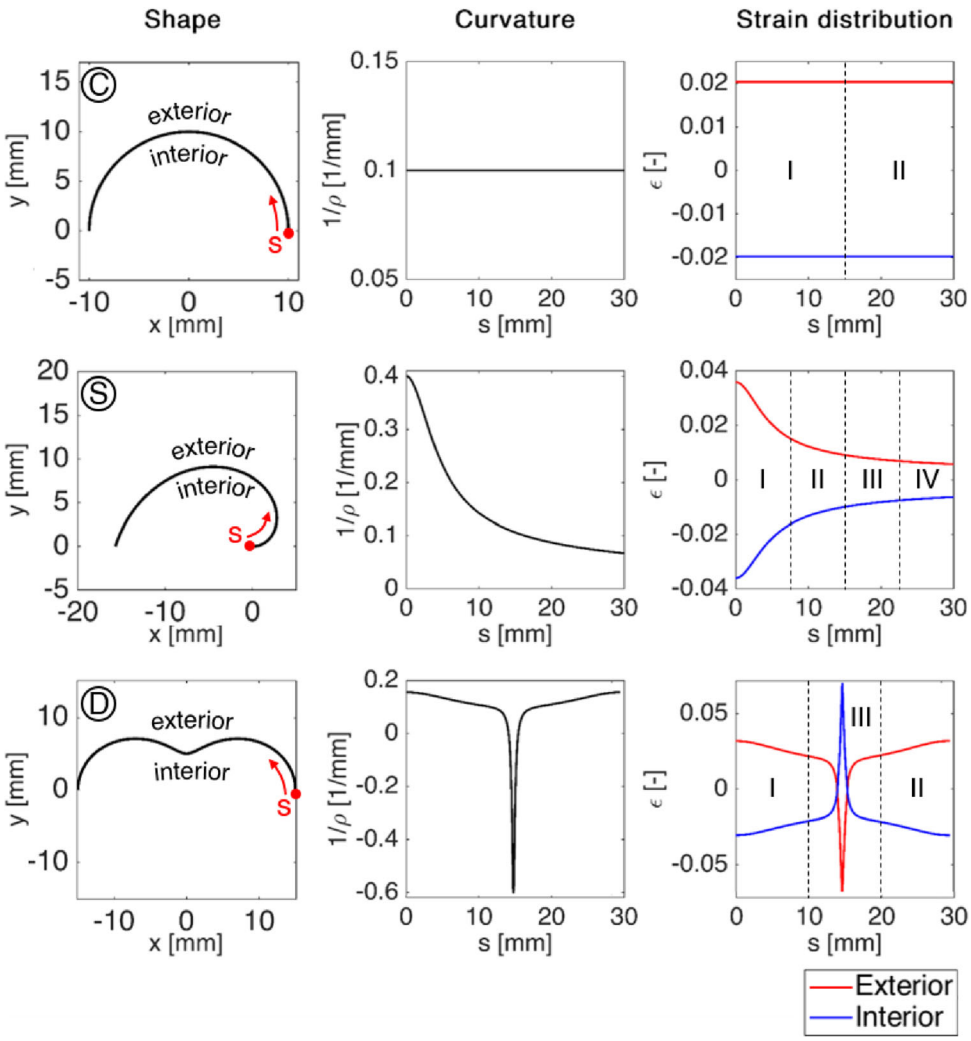

Figure 8 Representation in Cartesian coordinates of the three different curved geometries selected for the NiTi wires (left column). The values of curvature as a function of the axial coordinate of the wire are present in the middle column, while in the right column is plotted the distribution of strains along the innermost (interior) and outermost (exterior) sides of the curved wire, as a function of the position along the straightened wire.

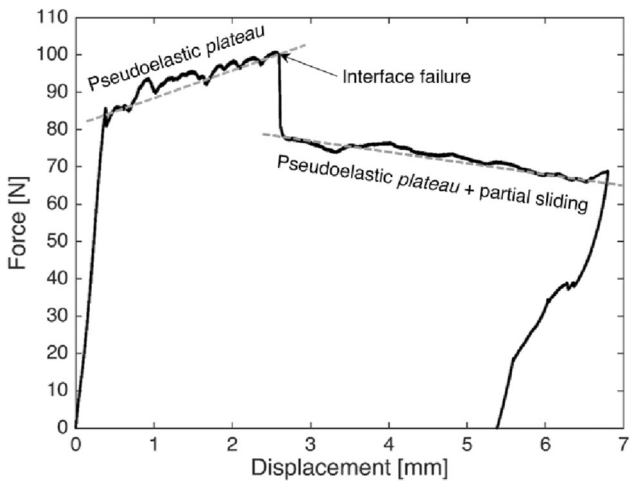

Figure 9 Sample pull-out test. The wire first displays a pseudoelastic response; after interface failure, the wire starts sliding within the epoxy matrix, while still retaining a sufficient level of stress to maintain the martensite partially detwinned.

than at intermediate ones: as temperature increases, η first decreases and then rises as T approaches the Tg of the epoxy resin. The plain sample, P, shows a monotonic increase in η with temperature, particularly past approximately 40 °C.

The effect of the frequency on η is the same for all samples: as the frequency increases η decreases. This is exemplified in Fig. 11 for the case of sample S. In the same figure, we observe once again the initial decrease in η from room temperature before the increase at higher temperatures. It is interesting to notice that this effect is zone dependent: it is especially evident for zone III and tends to become less evident as the frequency increases (from 25% for $f = 0.1$ Hz, down to 5% for $f = 5$ Hz). The zone dependency is also apparent in the different average values of η, as shown in Fig. 12. Zone III is confirmed

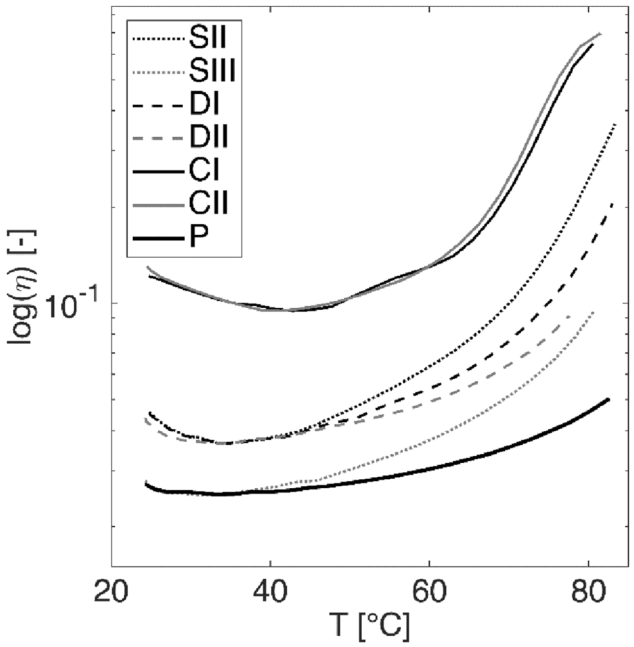

Figure 10 Values of η for the different samples as a function of temperature. All tests are carried out at 0.1 Hz.

as being the zone with highest damping, while zones I and II compete for the lower values.

Discussion

Factors affecting the damping of the NiTi wire

From a phenomenological point of view, dissipative effects observed in metallic materials can be explained by several anelastic relaxation phenomena, such as damping caused by the internal friction developed by defects, interfaces or because of thermoelastic effects [24]. Furthermore, considering the specific case of the NiTi alloy used for this study, nonlinear damping effects caused by the phase transformation must also be taken into account. Unlike the previously mentioned phenomena, these effects, also known as static damping, are dependent on amplitude [25].

While a comprehensive description of the microstructural phenomena underlying the dissipative effects observed in the alloy is beyond the scope of this study and can be found elsewhere [26], the results of the mechanical testing can still provide helpful insight into the various dependencies of the damping factor, as well as suggest effective strategies to tune and control it.

The marked amplitude dependency of the damping factor suggests a strong influence of the phase transformation on the dissipative phenomena, further confirmed when comparing the damping factor (Fig. 6) with the average areas of the partial hysteresis cycle (Fig. 13). As it can be seen, both quantities present similar trends in terms of amplitude and frequency dependency. Indeed, as the amplitude increases, the overall area of the partial hysteresis cycles will also increase, indicating a greater energy loss. This behaviour can also explain the effects of temperature and frequency, since the partial hysteresis cycles become narrower as either or both temperature and frequency increase.

However, this nonlinear damping effect is not sufficient to explain the effect of the pre-strain dependency.

In order to understand this phenomenon, we must take into account the stability of the different phases in various conditions [20]. As discussed therein, the wire used for this study presents a coexistence of R-phase and B2 austenite at room temperature. It has been shown [27] that the coexistence of different phases can promote dissipative phenomena in the material, increasing its overall damping capacity. If the surrounding thermal or mechanical conditions change, and the concentration of a particular phase increases, the level of coexistence will decrease, and the overall damping capacity will decrease with it.

Indeed, at low (1%L) or high (3%L) levels of pre-strain, there will be a higher stability respectively of the austenitic and martensitic phases, and the damping factor is in fact lower. Conversely, damping was found higher in an intermediate (2%L) condition where the phase transitions are in progress. This could also explain the difference between the tests performed on the loading and unloading *plateaux* (1%L vs 1%U). Since the mechanical energy required for the forward transformation is higher than that required for the reverse transformation, at 1%L the pre-strain is not enough to induce a significant formation of martensite, and the material is still mostly austenitic. Conversely, at 1%U, the material is undergoing the reverse (B19′- > *R*- > B2) transformation and, for the previously discussed reason, is in a condition favouring the coexistence of the different phases. This could therefore contribute to the observed higher damping.

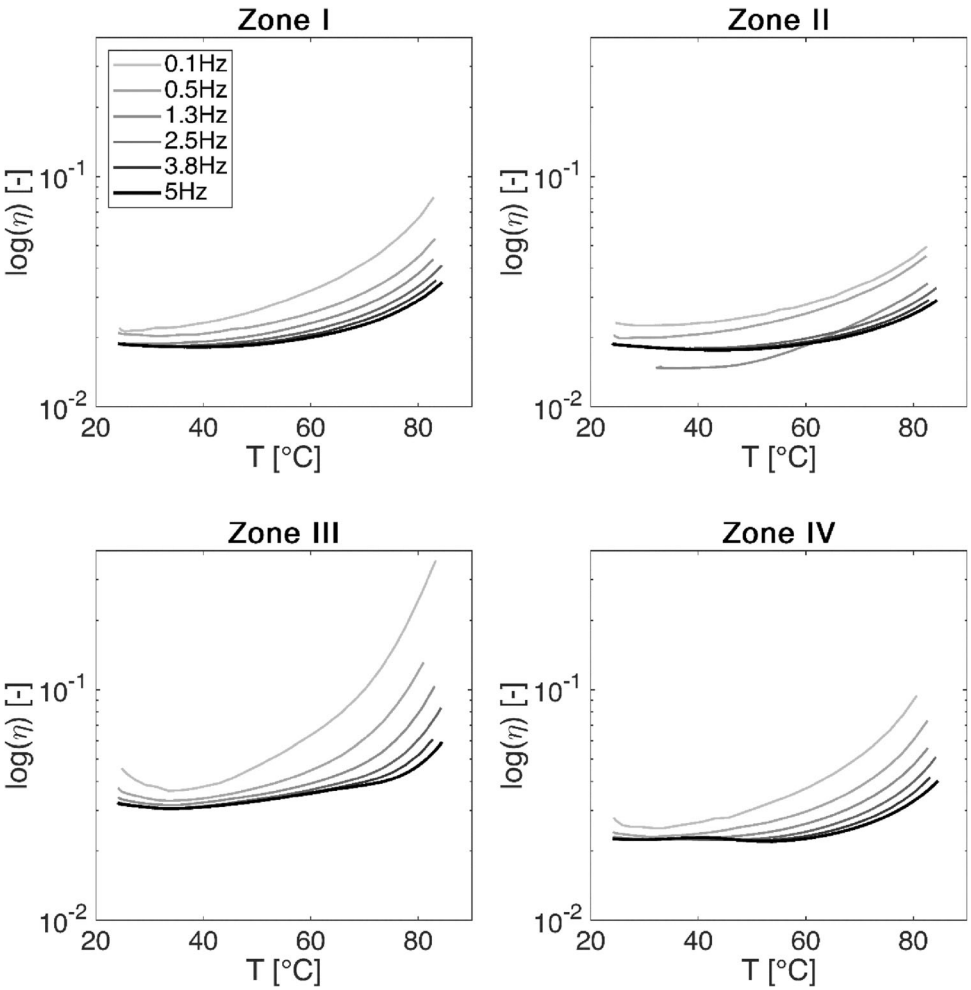

Figure 11 Results of DMA analysis of the different zones of sample S. Zone III has the highest damping values.

This phenomenon also affects the temperature dependency of the damping factor. Indeed, the austenitic phase will be more stable at higher temperatures. The lower levels of damping observed at higher temperature are thus also in agreement with the purposed explanation.

The origin of these effects becomes apparent when observing the hysteresis area of the partial cycles obtained in different dynamic conditions (Fig. 14). When decreasing cycle amplitude, a smaller portion of the material undergoes the phase transformation: the hysteresis area of the cycle is thus smaller, signalling that so is also the dissipated energy. On the other hand, increasing the frequency causes the cycles to become narrower, as a result of the thermoelastic phenomena occurring in increasingly adiabatic conditions because of the increasing loading speed. Once again, the smaller hysteresis is a mark of a reduction in the total dissipated energy per cycle.

Induction of damping factor gradients in the FGM

We have shown the pre-strain dependency of the damping factor, and that this effect can be controlled, and exploited to influence the graded damping response along the length of the polymer/metal composite sample.

By shape setting curved wires and then straightening them, we obtain fibres with a non-constant distribution of pre-strain, as discussed in "Design of FGM" section. This allows us to obtain regions where the material is "active", i.e. its damping capacity is enhanced, when compared to other regions. The pre-strain is then maintained by the epoxy resin matrix. This is the principle of the CPS approach.

When observing the mechanical response of the samples, the effects of the morphology-based pre-strain modulation are apparent. Samples with an asymmetrical pre-strain distribution (S) display

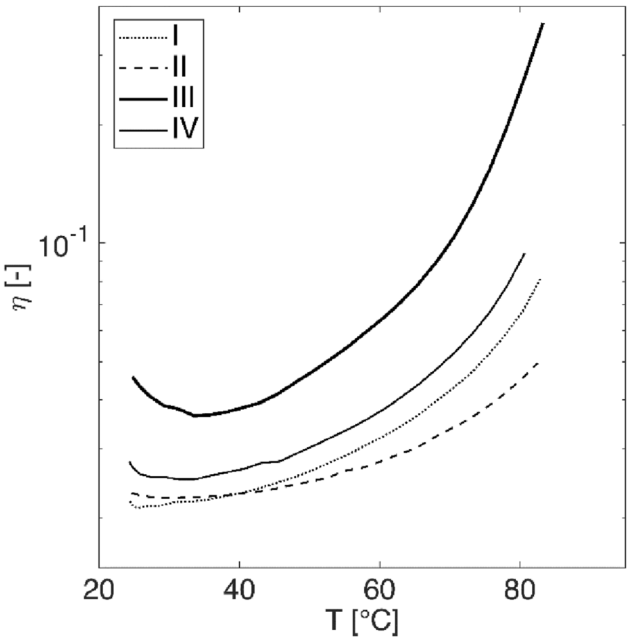

Figure 12 Detail of the zone dependency of the damping response for sample S. The zone with the most effective level of pre-strain (III) displays highest damping. All tests are carried out at 0.1 Hz.

asymmetrical response both in terms of overall η. When observing the effect of the dynamic load on different zones of sample S, the values of η are consistent with the observed effects of pre-strain on the NiTi wire: the highest level of damping is measured when the load is applied to zone III. This is a zone where straightening induced intermediate levels of pre-strain. As pre-strain decreases or increases from this condition, the observed damping of the composite is accordingly lower. In the light of the results of the tensile tests on the wires, showing the effects of phase mixture, we expect that the material in zone III will be characterised by higher levels of mixture. The actual-phase composition in this zone remains to be verified.

When evaluating the behaviour of the composite, it is worth to keep in mind the contribution of the epoxy matrix. In the samples, we always observe an increase in η as the temperature gradually moves towards the *T*g of the epoxy resin, which suggests that in these temperature ranges the matrix is the

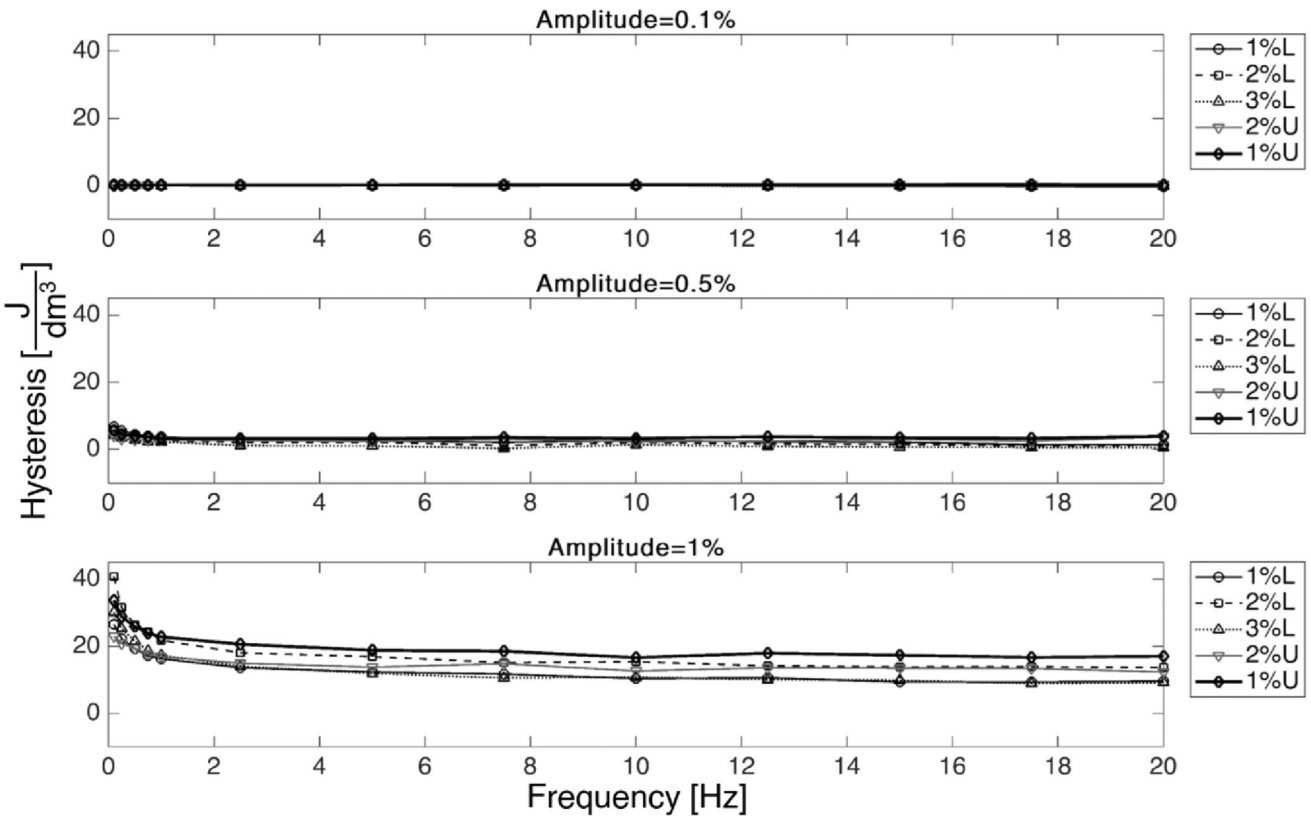

Figure 13 Average values of the hysteresis of the partial cycles of the NiTi wire as a function of amplitude, frequency and pre-strain level. The dependencies of the hysteresis area are qualitatively the same as those displayed by the damping factor, as shown in Fig. 6.

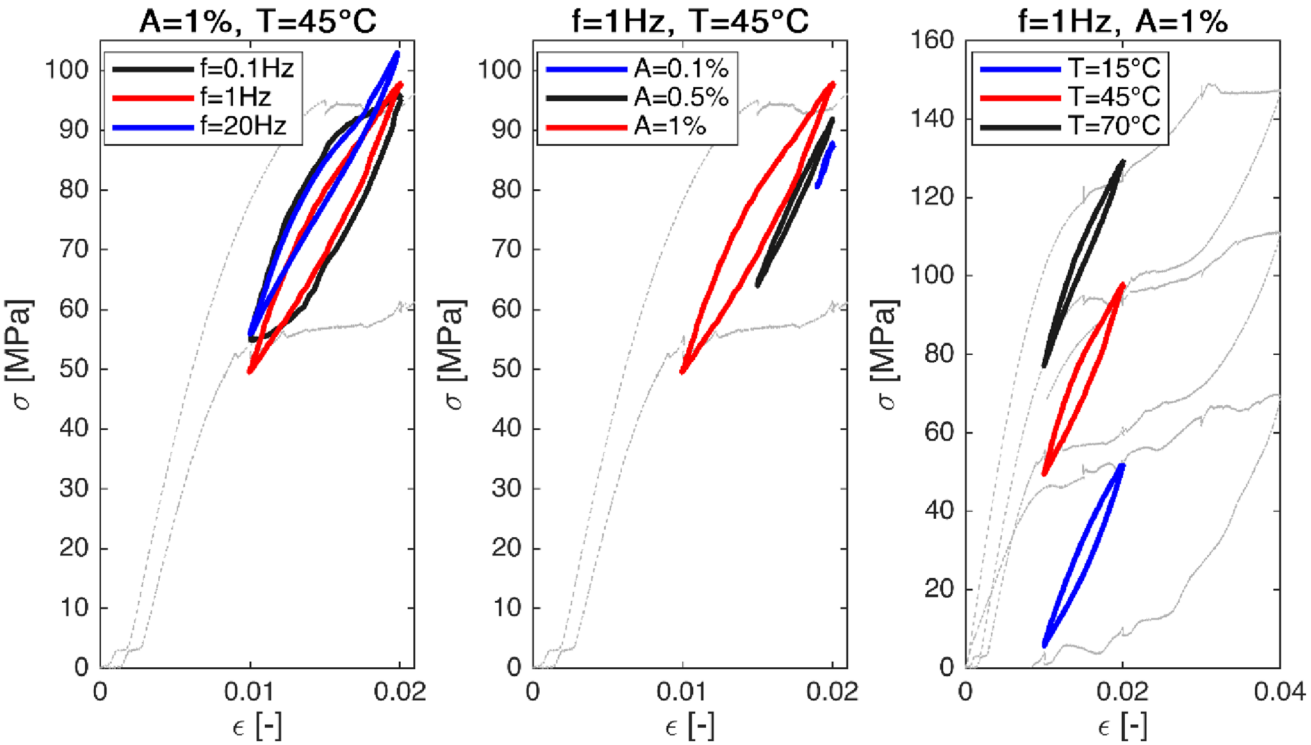

Figure 14 Partial hysteresis cycles in different testing conditions. Left: different frequencies, middle: Different amplitudes, right: different temperatures. The full quasi-static test is present in all conditions, in grey.

main contributor to the damping response of the composite.

Considering the effect of the metallic wire on the behaviour of the composite, an interesting indicator is the low versus high temperature response. As shown in "Mechanical characterisation of NiTi wire" section, the NiTi fibres display an exponential decrease in their damping factor for increasing temperatures. This is not true for the epoxy resin, whose damping factor increases for temperatures higher than 40 °C. In general, the combined properties will be a compromise between these opposing trends. In particular, we notice that a non-monotonic decreasing-increasing trend of η in the observed temperature range.

This temperature-driven effect is more manifest in the conditions where the material is "active". As a matter of fact, we observe this effect clearly for sample S, especially for zone III (compared to other zones—cf. Figure 12).

Besides the changes in the η-temperature trend caused by the level of pre-strain, there is also a frequency-dependent effect on η, visible specifically at the lower end of the investigated temperature range (Fig. 11). The explanation of this effect is once again in the relative contribution of the wire and matrix. If the frequency increases, the damping factor of the metallic wire decreases (cf. Figure 6) and its overall contribution to the response of the combined structure will decrease as well.

Conclusion

In the present study, we sought to investigate an innovative approach to induce a functional grading of the damping factor of a polymer–metal composite. We call it curvilinear pre-straining process, CPS.

We studied the damping behaviour of pseudoelastic NiTi wire and observed a pre-strain dependency. By exploiting shape-setting of the wire into curvilinear geometries, we were able to induce a controlled smooth distribution of pre-strain in the wire upon straightening. The measured difference in the mechanical response of the composite leads us to believe that we were successful in inducing a smoothly-varying damping response.

This approach and its results are promising in several applications where a continuous variation of the damping of a material is required, such as for the

development of highly-integrated components for sectors facing dynamical loads or inertial constraints (biomedical, aerospace, robotics, …). Considering the wide possibilities allowed by the shape setting process of SMAs, the distribution of the damping factor is easy to control in order to meet the desired requirements. This tuning can be carried out during the material design, but it should also be possible to adapt it dynamically, by exploiting the temperature dependency of the phenomenon. In addition to the functional grading, this kind of composite could also be activated by heating/cooling the metallic wire, for example, through an electrical current.

For this kind of application, a limitation of the present study consists in the evaluation of the effects of the epoxy resin. Continuum modelling of the composite, taking into account the interfacial effects and their temperature dependence, could increase the understanding of the contribution of the resin to the damping behaviour, and its interplay with the metallic wire. In order to carry out this type of study, it will also be necessary validate a constitutive model for the interface identifying its parameters. Furthermore, as shown in the discussion, a higher value of Tg could allow a wider range of temperature control of the wire, without approaching areas where the behaviour of the resins starts to become preponderant in the overall response of the composite.

Furthermore, our work could certainly benefit from a better quantitative evaluation of the effects of the different dissipative phenomena occurring in the metallic alloy. While we were able to observe a coherent behaviour between the pre-strain dependency of η and the damping factor of the composite, an optimised tuning and control of its mechanical response will require more in-depth characterisation of the effects of CPS on damping mechanisms other than mechanical hysteresis. In particular, the bending behaviour of the wire is of interest [28].

Another important issue that will require further consideration is that of the fatigue resistance of the polymer–metal interface. While the interface was sufficiently stable to hold the pre-strain of the wire, and maintain it during mechanical testing, a more comprehensive study of long-term fatigue phenomena should be carried out. The effects of temperature on the fatigue life of the composite are also of interest.

Finally, the viscoelastic behaviour of the epoxy resin should be investigated, to evaluate the evolution in time of the pre-strain of the fibres caused by the viscoelasticity of the resin. It has been observed that, after several weeks on the shelf, the samples showed no signs of curving. (Hence the resin was still able to at least maintain the metallic fibres straight.) However, the effects of this phenomenon on the damping efficiency of the composite remains to be determined, as well as the effects of interface phenomena.

Despite these issues, we believe that the present study demonstrates how trying to pursue a synergistic approach between material shape and function can lead to promising results in the field of fabricating functionally graded polymer/metal functionalised structural materials.

Acknowledgements

The authors would like to thank Enrico Bassani from CNR ICMATE for his technical assistance in the fabrication of the fixtures for the thermal annealing, and the fixture for the curing of the composites. This study was not funded by any sources.

Author contributions

JR did conceptualization, investigation, writing—original draft. LG performed writing—review & editing. FL provide writing—review & editing. FV done writing—review & editing. FBV gave supervision. SP did conceptualization and supervision.

Funding

Open access funding provided by Consiglio Nazionale Delle Ricerche (CNR) within the CRUI-CARE Agreement.

Data and code availability

The data used for this study will be made available on request.

Declarations

Conflict of interest The authors declare no conflicts of interest.

Ethical approval Not applicable.

Supplementary Information: The online version contains supplementary material available at https://doi.org/10.1007/s10853-023-08612-2.

References

[1] Atarashiya T, Ishida K, Nagai Y (1992) Fundamental study on relaxation of thermal stress for high-temperature material by tailoring the graded structure. Ceram Trans 34:141–148

[2] Kumar S, Murthy Reddy KVVS, Kumar A, RohiniDevi G (2013) Development and characterization of polymer-ceramic continuous fiber reinforced functionally graded composites for aerospace application. Aerosp Sci Technol 26(1):185–191

[3] Shahriari B, Safari M (2020) Stress analysis of FGM rotating disk subjected to mechanical and thermal loads in aircraft gas turbine engine. Mech Adv Compos Struct 7(1):1–13

[4] Müller E, Drašar Č, Schilz J, Kaysser WA (2003) Functionally graded materials for sensor and energy applications. Mater Sci Eng A 362(1–2):17–39

[5] Shimazaki Y, Nozu S, Inoue T (2016) Shock-absorption properties of functionally graded EVA laminates for footwear design. Polym Test 54:98–103

[6] Udupa G, Rao SS, Gangadharan KV (2014) Functionally graded composite materials: an overview. Procedia Mater Sci 5:1291–1299

[7] Ebhota WS, Karun AS, Inambao FL (2016) Centrifugal casting technique baseline knowledge, applications, and processing parameters: overview. Int J Mater Res 107(10):960–969

[8] Zhu J, Lai Z, Yin Z, Jeon J, Lee S (2001) Fabrication of ZrO_2-NiCr functionally graded material by powder metallurgy. Mater Chem Phys 68(1–3):130–135

[9] Nam HK, Keun HK (1994) Deposition of SiC/C functionally gradient materials by chemical vapour deposition. J Korean Cryst Growth Cryst Technol 4(3):262–275

[10] Zhou ZJ, Song SX, Du J, Zhong ZH, Ge CC (2007) Performance of W/Cu FGM based plasma facing components under high heat load test. J Nucl Mater 363–365(1–3):1309–1314

[11] Khoddami AM, Sabour A, Hadavi SMM (2007) Microstructure formation in thermally-sprayed duplex and functionally graded NiCrAlY/Yttria-stabilized Zirconia coatings. Surf Coatings Technol 201(12):6019–6024

[12] Kim SK, Yoo HJ (1998) Formation of bilayer Ni-SiC composite coatings by electrodeposition. Surf Coatings Technol 108–109:564–569

[13] Zhang B, Jaiswal P, Rai R, Nelaturi S (2018) Additive manufacturing of functionally graded material objects: a review. J Comput Inf Sci Eng 18:4

[14] Saleh B et al. (2020) 30 Years of functionally graded materials: an overview of manufacturing methods, applications and future challenges. *Compos Part B Eng*., 201

[15] Oxman N (2010) Structuring materiality: design fabrication of heterogeneous materials. Archit Des 80(4):78–85

[16] Van Humbeeck J, Chandrasekaran M, Delaey L (1991) Shape memory alloys: materials in action. *Endeavour*

[17] Burkes DE, Moore JJ (2007) Microstructure and kinetics of a functionally graded NiTi-TiC*x* composite produced by combustion synthesis. J Alloys Compd 430(1–2):274–281

[18] Gangil N, Siddiquee AN, Mufazzal S, Muzakkir SM, Maheshwari S (2021) Shape memory alloy based NiTi reinforced functionally graded material for vibration damping. Proc Inst Mech Eng Part L J Mater Des Appl 235(12):2771–2782

[19] Ghasali E, Baghchesaraee K, Orooji Y (2020) Study of the potential effect of spark plasma sintering on the preparation of complex FGM/laminated WC-based cermet. *Int J Refract Met Hard Mater*. 92

[20] Romanò J, Lazzari F, Garavaglia L, Pittaccio S (2022) Short duration heat treatments before aging increase mechanical hysteresis of pseudoelastic NiTi alloy. J Mater Eng Perform 31(7):5478–5484

[21] Rossi S, Deflorian F, Pegoretti A, D'Orazio D, Gialanella S (2008) Chemical and mechanical treatments to improve the surface properties of shape memory NiTi wires. Surf Coatings Technol 202(10):2214–2222

[22] Ugural AC, Fenster SK (2011) Advanced mechanics of materials and applied elasticity. Pearson Education

[23] DiFrancia C, Ward TC, Claus RO (1996) The single-fibre pull-out test. 1: review and interpretation. Compos Part A Appl Sci Manuf 27(8):597–612
[24] Nowick AS (1953) Internal friction in metals. Prog Met Phys 4:1–70
[25] Ritchie ZL, Pan IG (1991) High damping metals and alloys. Metall Trans A 22:607–616
[26] Liu Y, Van Humbeeck J (1997) On the damping behaviour of NiTi shape memory alloy. J Phys IV JP 7:5
[27] Zhang J, Perez RJ, Wong CR, Lavernia EJ (1994) Effects of secondary phases on the damping behaviour of metals, alloys and metal matrix composites. Mater Sci Eng R 13(8):325–389
[28] Ostadrahimi A, Arghavani J, Poorasadion S (2015) An analytical study on the bending of prismatic SMA beams. Smart Mater Struct 24:12